energies

MDPI

Article

Machine Learning-Assisted Prediction of Ambient-Processed Perovskite Solar Cells' Performances

Dowon Pyun [1,†], Seungtae Lee [1,†], Solhee Lee [1,†], Seok-Hyun Jeong [1], Jae-Keun Hwang [1], Kyunghwan Kim [1], Youngmin Kim [2], Jiyeon Nam [1], Sujin Cho [1], Ji-Seong Hwang [1], Wonkyu Lee [1], Sangwon Lee [2], Hae-Seok Lee [2], Donghwan Kim [1] and Yoonmook Kang [2,*]

[1] Department of Materials Science and Engineering, Korea University, Seoul 02841, Republic of Korea; dowon0212@korea.ac.kr (D.P.); tmdxo12344@korea.ac.kr (S.L.); rnlxlsla@korea.ac.kr (S.L.); jsh7983@korea.ac.kr (S.-H.J.); hjk1024@korea.ac.kr (J.-K.H.); kaekim37@korea.ac.kr (K.K.); njy9964@korea.ac.kr (J.N.); csj9528@korea.ac.kr (S.C.); gomthang@korea.ac.kr (J.-S.H.); dldnjsrb@korea.ac.kr (W.L.); solar@korea.ac.kr (D.K.)

[2] Graduate School of Energy and Environment (KU-KIST Green School), Korea University, Seoul 02841, Republic of Korea; young970919@korea.ac.kr (Y.K.); basil1997@korea.ac.kr (S.L.); lhseok@korea.ac.kr (H.-S.L.)

* Correspondence: ddang@korea.ac.kr; Tel.: +82-2-3290-3713

† These authors contributed equally to this work.

Abstract: As we move towards the commercialization and upscaling of perovskite solar cells, it is essential to fabricate them in ambient environment rather than in the conventional glove box environment. The efficiency of ambient-processed perovskite solar cells lags behind those fabricated in controlled environments, primarily owing to external environmental factors such as humidity and temperature. In the case of device fabrication in ambient environments, relying solely on a single parameter, such as temperature or humidity, is insufficient for accurately characterizing environmental conditions. Therefore, the dew point is introduced as a parameter which accounts for both temperature and humidity. In this study, a machine learning model was developed to predict the efficiency of ambient-processed perovskite solar cells based on meteorological data, particularly the dew point. A total of 238 perovskite solar cells were fabricated, and their photovoltaic parameters and dew points were collected from March to December 2023. The collected data were used to train various tree-based machine learning models, with the random forest model achieving the highest accuracy. The efficiencies of the perovskite solar cells fabricated in January and February 2024 were predicted with a MAPE of 4.44%. An additional Shapley Additive exPlanations analysis confirmed the significance of the dew point in the performance of perovskite solar cells.

Keywords: ambient processed; perovskite solar cells; dew point; artificial intelligence; machine learning

Citation: Pyun, D.; Lee, S.; Lee, S.; Jeong, S.-H.; Hwang, J.-K.; Kim, K.; Kim, Y.; Nam, J.; Cho, S.; Hwang, J.-S.; et al. Machine Learning-Assisted Prediction of Ambient-Processed Perovskite Solar Cells' Performances. *Energies* **2024**, *17*, 5998. https://doi.org/10.3390/en17235998

Academic Editors: Hubert Seigneur and Kristopher Davis

Received: 4 November 2024
Revised: 26 November 2024
Accepted: 27 November 2024
Published: 28 November 2024

1. Introduction

Perovskite solar cells have attracted significant attention as a next-generation photovoltaic technology due to their high efficiency [1], bandgap tunability [2], and high absorption coefficients [3]. Over the past decade, their efficiency has notably increased from 3.81% [4] in 2009 to 26.7% in 2024 [5], and have now almost approached the highest reported efficiency of silicon solar cells. With the rapid growth in their efficiency, perovskite solar cells have also been integrated into perovskite/silicon tandem solar cells [6–10], which are expected to surpass the theoretical efficiency limits of single-junction solar cells. Traditional solution-based methods such as spin-coating are generally utilized for perovskite formation [11,12]. The dry deposition of perovskite has also emerged as a promising method recently [13–15]. However, most of the high-efficiency perovskite solar cells reported have been achieved at the lab scale with small active areas (less than 0.1 cm^2) under controlled environments [16] such as glove boxes filled with inert gas. This is attributed to the high sensitivity of perovskite materials to external environmental conditions such as moisture.

However, for the future commercialization of large-scale perovskite solar cells, fabrication techniques must advance beyond conventional glove box processing to allow for fabrication in an ambient environment. Thus, many research groups are working to enhance the performance and stability of ambient-environment-processed perovskite solar cells using various strategies [17–22]. Unfortunately, those fabricated in ambient environments generally exhibit a relatively low performance [23]. An effective method to mitigate the influence of the external environment on the performance of perovskite solar cells to achieve an efficiency of exceeding 25% under ambient atmosphere is still lacking. It is clear that ambient environments contain various elements that can adversely affect perovskite absorbers such as humidity, temperature, and light [24–27]. A high relative humidity, in particular, disrupts the nucleation process during precursor spin-coating and annealing, leading to negative impacts on the surface morphology of the perovskite film and the device's performance [23,28,29]. Moreover, it accelerates the irreversible decomposition of perovskite into lead iodide [30]. Such degradation caused by the ambient environment reduces the reproducibility of the fabricated devices, making it more difficult to predict their photovoltaic performance.

In this work, we aim to construct a model to predict the efficiency of devices fabricated under ambient environmental conditions. Recently, artificial intelligence (AI) has been applied to predict the efficiency of perovskite solar cells under varying external environmental conditions using machine learning [31–33]. Most prediction models have only focused on relative humidity among various external environmental factors under precisely controlled conditions. However, in the case of device fabrication in ambient environments, we argue that relying solely on a single parameter, such as temperature or humidity, is insufficient for accurately characterizing environmental conditions. For instance, Ko et al. [34] reported that different thin film qualities were obtained even at the same relative humidity. To achieve a more accurate characterization of ambient environmental conditions, therefore, the dew point was introduced as a parameter that accounts for both temperature and humidity. The dew point is a parameter proportional to both relative humidity and temperature, which will be discussed more in the following Discussion Section. To the best of our knowledge, this is the first attempt to use dew points to predict the efficiency of perovskite solar cells. Our prediction provides guidelines for fabricating ambient-processed perovskite solar cells and is anticipated to contribute significantly to the future commercialization and upscaling of perovskite solar cells

2. Materials and Methods

Fluorine-doped tin oxide (FTO) substrates were purchased from Pilkington. Acetone, ethanol, and 2-propanol (99.7% purity; HPLC grade) were purchased from Duksan. N,N-dimethylformamide (anhydrous, 99.8% purity), dimethyl sulfoxide (anhydrous, 99.9% purity), diethyl ether (anhydrous, 99.7% purity), chlorobenzene (anhydrous, 99.8% purity), Acetonitrile (anhydrous, 99.8% purity), bis (trifluoromethane) sulfonimide lithium salt (Li-TFSI, 99.95% purity, trace metal basis), and 4-tert-butylpyridine (98% purity) were purchased from Sigma-Aldrich. Methylammonium iodide (99.99% purity) was purchased from Greatcell Solar Materials. 2,2′,7,7′-tetrakis-(N,N-di-4-methoxyphenylamino)-9,9′-spiro bifluorene (spiro-OMeTAD, 99% purity) was purchased from Lumtec. Lead iodide (PbI_2, 99.99% purity, trace metal basis, for perovskite precursor) was acquired from Tokyo Chemical Industry (TCI, Chuo-ku, Japan).

FTO glass substrates were cleaned using acetone, ethanol, and 2-propanol sequentially in an ultrasonicator for 15 min. The cleaned FTO substrate was then exposed to UV–ozone for 30 min with UV-ozone cleaner (AH1700 model, AHTECH LTS Co., Ltd., Anyang-si, Gyeonggi-do, Republic of Korea). SnO_2 was deposited by RF magnetron sputtering, as optimized in our previous study [11]. A $MAPbI_3$ precursor solution was prepared by dissolving PbI_2 (1 mM), methyl ammonium iodide (172 mg), and dimethyl sulfoxide (71 μL) in a dimethylformamide solvent (636.6 μL). Diethyl ether was dropped during spin coating, and the substrate was dried on a hot plate at 60 °C for 1 min, followed by 100 °C

for 5 min. The fabrication of the perovskite absorber layer is identical to that reported in our previous research [10,35,36]. For the hole transportation layer (HTL) coating, the spiro-OMeTAD powder was dissolved in 4-tert-butylpyridine (28.8 μL), Li-TFSI (520 mg in 1 mL of acetonitrile), and chlorobenzene (1 mL) solutions. This solution was applied to the substrate, and a thin layer with 200 nm thickness was formed by spin coating. Finally, 100 nm of Au was deposited by thermal evaporation.

The photovoltaic performance of the perovskite solar cells was measured using a solar simulator (WACOM WXS-155S10 class AAA) with 100 mW/cm^2 irradiation using a Xe lamp. Modulated reference Si solar cells were used for calibration before the measurements. The devices were evaluated using shadow masks with an aperture size of 0.075 cm^2. The scan voltage setting time was 40 mV/s.

3. Results and Discussion

Significant variations in precipitation levels exist regionally and seasonally. For instance, South Korea experiences concentrated rainfall in July and August, whereas Portugal receives less rainfall during the same period. As precipitation is directly related to humidity, the efficiency of ambient-environment-processed perovskite solar cells varies depending on the location and timing of their fabrication. Experimentally, perovskite films fabricated in an ambient environment under high-humidity conditions (>40%) exhibited surface stains (Figure S1) despite an air conditioner and dehumidifier being in operation. These stains are the result of the non-uniform crystallization of a perovskite precursor. Since the perovskite precursor and final thin films are exposed to the external environment during the spin-coating and annealing steps, it is clear that external environmental factors significantly influence not only the crystallization step but also the device's properties.

In this study, perovskite solar cells were fabricated, and their photovoltaic parameters and meteorological data at the time of fabrication were collected from March to December 2023. The collected data were used to train a machine learning model to predict the device's efficiency at specific dew points. The dew point for a given relative humidity (RH) and air temperature (T) can be calculated using the Magnus formula [34].

$$\text{Dew Point } (^\circ\text{C}) = \text{f(RH, T)} = \frac{243.12 \times \left(\ln\left(\frac{\text{RH}}{100}\right) + \frac{17.62 \times \text{T}}{243.12 + \text{T}}\right)}{17.62 - \left(\ln\left(\frac{\text{RH}}{100}\right) + \frac{17.62 \times \text{T}}{243.12 + \text{T}}\right)}$$

The formula shows that the dew point is a parameter proportional to relative humidity and temperature. Figure 1 shows the flowchart for the dew-point-based efficiency prediction process. The detailed processes are discussed in the following sections.

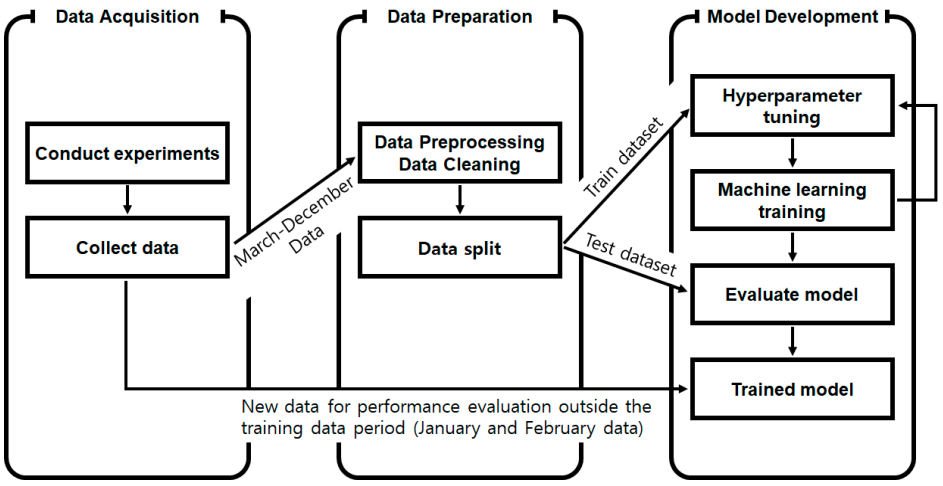

Figure 1. Entire flowchart for dew-point-based efficiency prediction in this study.

3.1. Data Collection

In this work, to investigate the effect of external environments on the perovskite layer, perovskite solar cells were fabricated with structure of FTO/SnO_2/$MAPbI_3$/spiro-OMeTAD/Au. Their photovoltaic parameters and meteorological data at the time of fabrication were collected over a year (March–December 2023). These data were used to train a machine learning model to predict the device's efficiency at specific dew points. Dew points were collected using two methods: (1) laboratory measurements and (2) data from the Korea Meteorological Administration (KMA). Relative humidity and temperature during fabrication were recorded using a thermohygrometer in our laboratory (Figure S2). Dew points were calculated using the Magnus equation (Equation (1)). Dew points were also obtained from the KMA (www.weather.go.kr, accessed on 29 December 2023). A linear relationship was confirmed between the laboratory and KMA dew points (Figure S3). In both cases, higher dew points were observed during summer, and lower dew points were observed during winter, validating the feasibility of using KMA-reported dew points. Given its broader applicability, the KMA-reported dew points were used as input data for the machine learning.

Figure 2 shows the photovoltaic parameters plotted against dew points. Additionally, only the external environment was varied during the perovskite film fabrication, while all other steps, including measurements, were conducted under identical standard test conditions. Device performance tended to decrease with increasing dew points, consistent with previous research indicating high humidity's adverse effects on perovskite solar cells. One important observation is that the decline in the open-circuit voltage (V_{OC}) and fill factor (FF) was more significant than the decline in the short-circuit current density (J_{SC}). This behavior is consistent with the effect of defect density on the photovoltaic performances of thin-film solar cells. Related findings have been reported in various studies, including those on CdTe solar cells [37–40] and perovskite solar cells [41–43]. For instance, Chouhan et al. [43] reported simulation results demonstrating that increases in interface and bulk defect density significantly impact V_{OC} and FF. In fact, many groups employ interface [11] and bulk [44] passivation technologies to mitigate drops in the performance of perovskite absorbers.

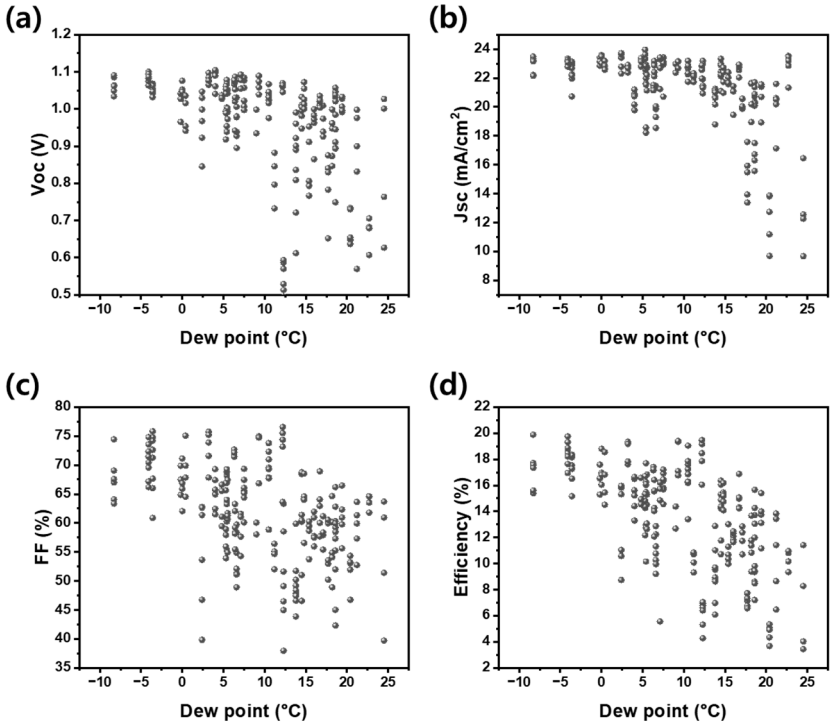

Figure 2. Photovoltaic parameters of perovskite solar cells fabricated under various dew points. A total of 238 devices were collected and measured. (**a**) V_{OC}, (**b**) J_{SC}, (**c**) FF, and (**d**) efficiency.

Additional analyses were conducted using the Solar Cell Capacitance Simulator (SCAPS-1D) simulation program [45]. The bulk defect density in $MAPbI_3$ was controlled to investigate how it affects device performance. The structure of the device used in the simulation is identical to that of the fabricated device, specifically, FTO/SnO2/$MAPbI_3$, spiro-OMeTAD/Au. The input parameters are summarized in Table S1. Those parameters are based on those reported in reference [46] and the experimental values confirmed in our previous research, such as a bandgap of 1.52 eV for $MAPbI_3$ [10]. As a result, an efficiency of about 20% was obtained at a density of 5×10^{15} cm^{-3}. Considering that a density level of 8×10^{15} cm^{-3} was confirmed in our previous study [11], it was confirmed that the simulation results align well with the experimental data. As shown in Figure 3, an increasing defect density led to a deterioration in the performance of perovskite solar cells, particularly in V_{OC} (Figure 3b) and FF (Figure 3d).

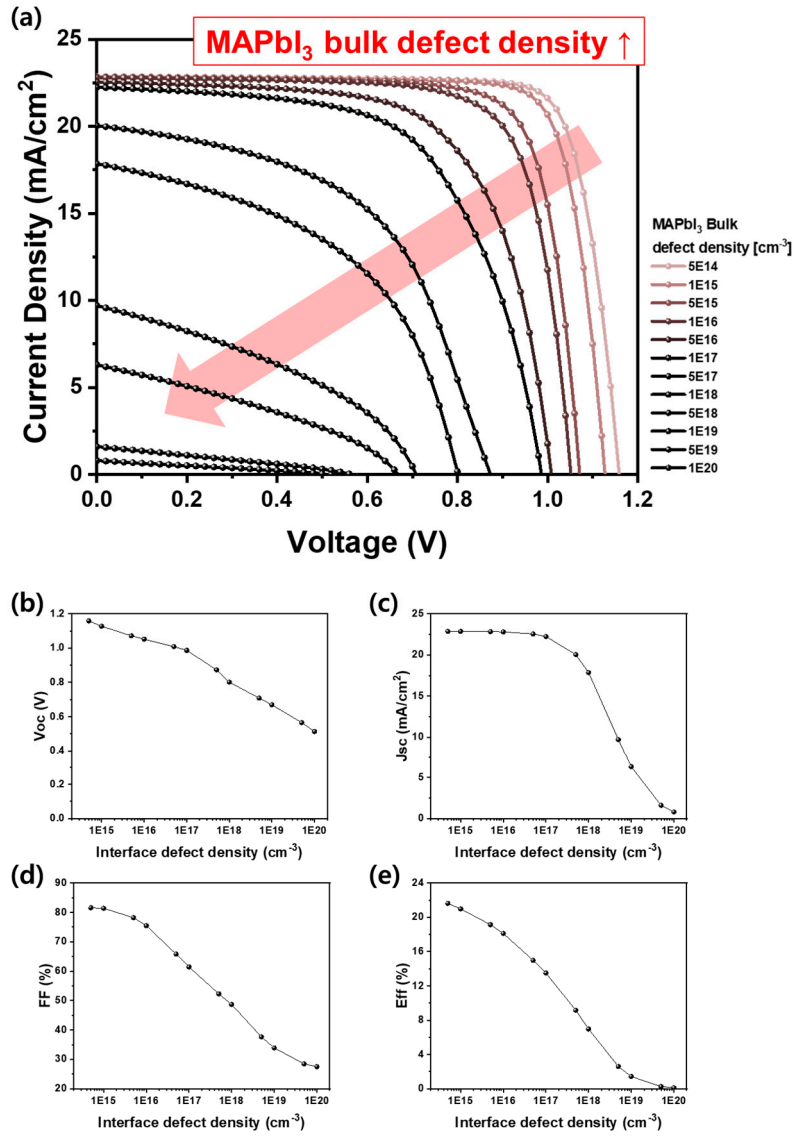

Figure 3. Effects of bulk defect density in $MAPbI_3$ simulated with SCAPS-1D. (**a**) J-V curve, (**b**) V_{OC}, (**c**) J_{SC}, (**d**) FF, and (**e**) efficiency. The red arrow in (**a**) indicates an increase of bulk defect density in $MAPbI_3$.

Since defects located in the perovskite layer act as a recombination site, this defect-mediated recombination leads to reduced carrier collection. Therefore, deteriorated photovoltaic parameters were observed, as the number of defects increases. This trend, similar

to that observed in Figure 2, indicates that the dew point affects the perovskite absorber during fabrication, suggesting its potential as a predictor of perovskite solar cell performance. In fact, initially, at the low dew point, the data exhibit relatively similar trends; however, at higher dew points, the distribution among data points increased, deviating from the simulation results. This inconsistency between the experiment data and the simulation results may be attributed to the low stability of devices fabricated under high dew point conditions. Devices fabricated under high-dew-point conditions exhibited significantly deteriorated photovoltaic performances with low stabilities, resulting in considerable distribution between data points even fabricated under the same dew point.

Combining the experimental data and simulation results, we made the following conclusions. Perovskite films crystallized in high-dew-point conditions tend to incorporate numerous defects. These internal bulk defects lead to degraded photovoltaic performances. As a result, perovskite films fabricated under high-dew-point conditions result in deteriorated photovoltaic performances.

3.2. Machine Learning

Due to the high sensitivity of perovskite material to various external factors during ambient atmosphere fabrication, efficiency deviations occurred even within the same batch. Thus, data pre-processing was required for more accurate predictions. Outliers were excluded from the experimental data, retaining only data within a 1.5% range of the batch's average efficiency value. This process resulted in 165 data points for constructing the training and testing datasets.

The dataset was divided into training and test subsets in an 8:2 ratio, employing 10-fold cross-validation to train the models. This method partitions the dataset into ten equally sized subsets, where nine subsets are used for training, and the remaining subset serves as the test set. The process is repeated 10 times, with each of the ten subsets being used exactly once as the test set. This approach enhances model learning efficiency, reduces overfitting risk, and improves validation confidence, especially with limited data.

Model performance was validated using the test dataset, with predictive capabilities assessed through the coefficient of determination (R^2), root mean square error (RMSE), and mean absolute percentage error (MAPE). These metrics are crucial for evaluating model precision and reliability. Table 1 lists the calculation methods used for each performance metric.

Table 1. Performance metrics with equations for evaluating machine learning predictions. For more detail, n is the total number of observations, y_i is the actual observed value for the ith observation, $\hat{y}_i$ is the predicted value for the ith observation by the machine learning model, and $\overline{y}$ is the mean of the actual observed values.

Performance Metrics	Equation
R^2	$1 - \frac{\sum_{i=1}^{n}(y_i - \hat{y}_i)}{\sum_{i=1}^{n}(y_i - \overline{y})}$
RMSE	$\sqrt{\frac{1}{n}\sum_{i=1}^{n}(y_i - \hat{y}_i)^2}$
MAPE	$\frac{1}{n}\sum_{i=1}^{n}\frac{\lvert\hat{y}_i - y_i\rvert}{y_i} \times 100$

The model selection process emphasized tree-based models, based on Grinsztajn et al. [47], indicating that tree-based ensemble methods, such as bagging and boosting, are more effective than deep learning models on tabular data and that deep learning struggles to detect patterns within small datasets. Consequently, five distinct machine-learning algorithms were adopted: the decision tree regressor (DT), random forest regressor (RF), gradient boosting regressor (GB), light gradient boosting machine (LightGBM), and adaptive boosting regressor (AdaBoost). The best model was selected through performance

comparison after hyperparameter optimization. Table 2 lists the prediction errors for each model's efficiency.

Table 2. Prediction accuracy with each machine learning model.

Model	R^2	RMSE [%]	MAPE [%]
RF	0.9349	0.9434	5.14
GB	0.9314	0.9683	5.25
DT	0.9292	0.9638	5.29
AdaBoost	0.8628	1.3690	7.6
LightGMB	0.8160	1.5856	9.61

The random forest model outperformed others, with the highest R^2 value of 0.9349 and the lowest RMSE and MAPE values of 0.9434% and 5.14%, respectively. Therefore, random forest was selected as the prediction model. Figure 4a shows predicted versus actual efficiency values for the training and test sets, confirming the model's accuracy and ability to avoid overfitting (see Figure S4 for remaining photovoltaic parameters).

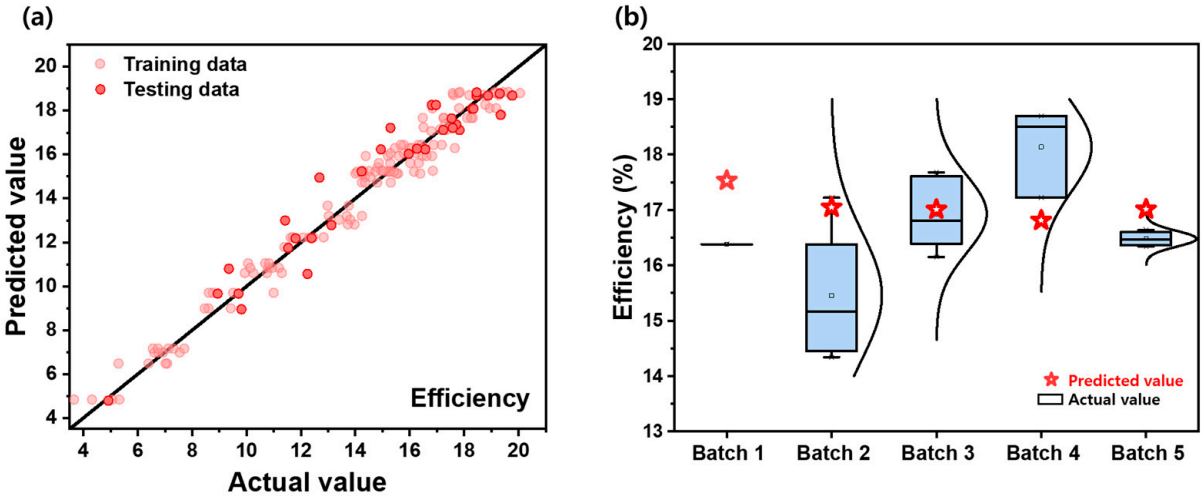

Figure 4. Prediction results using the trained random forest model. (**a**) Graph showing the actual values on the *x*-axis and the predicted values on the *y*-axis; closer alignment to the y = x line indicates more accurate predictions. The light red dots represent training dataset predictions, while dark red dots represent test dataset predictions. (**b**) The efficiency distribution (box chart) of the fabricated devices in January and February 2024, with predicted results (red stars) obtained using our model.

The performance of perovskite solar cells fabricated in January and February 2024 was compared with model predictions to validate the model. Five experiments over two months showed that the predicted efficiencies (red stars in Figure 4b) fell within the actual efficiency range, achieving an MAPE of 4.44%.

This outcome is significant considering Korea's climate conditions, with high dew points in July and August and low dew points in January and February. The model, trained on data from March to December (periods typically characterized by higher dew points), effectively predicted solar cell parameters even during low dew point seasons, demonstrating reliable predictions across diverse environmental conditions; this highlights its potential as a valuable tool for guiding the fabrication of perovskite solar cells in real-world settings.

The complexity of tree-based ensemble models necessitates additional methodologies for interpretability. Shapley Additive exPlanations (SHAPs) are one such tool, facilitating model interpretation [48–50]. This study used SHAPs to identify key factors influencing perovskite solar cell efficiency. The graph on the left in Figure 5a shows feature importance,

revealing the impact of various factors on the power conversion efficiency (PCE). The feature importance (average SHAP value) of the dew point is 2.63, higher than that of the other values, indicating that the dew point is more important than other factors in predicting the PCE; this suggests that, in real-world production environments, the influence of dew point may outweigh other factors. The graph on the right in Figure 5a shows a violin plot, visually representing the SHAPs distribution for each sample. The plot thickness reflects the concentration of points while utilizing a color gradient, where red indicates high feature values and blue represents low feature values. The graph shows a clear tendency for the color of the violin plot, representing the dew point, to shift from red to blue as the SHAPs value increases; this indicates that an increase in the dew point negatively impacts efficiency. The negative relationship between dew point and efficiency is even more evident in Figure 5b, which suggests that performing the process at a dew point below 13 °C is beneficial for achieving high-efficiency ambient-processed perovskite solar cells. Furthermore, as shown in Figure S5, the threshold derived from SHAP analysis aligns with the threshold obtained from model predictions, validating the consistency of these findings.

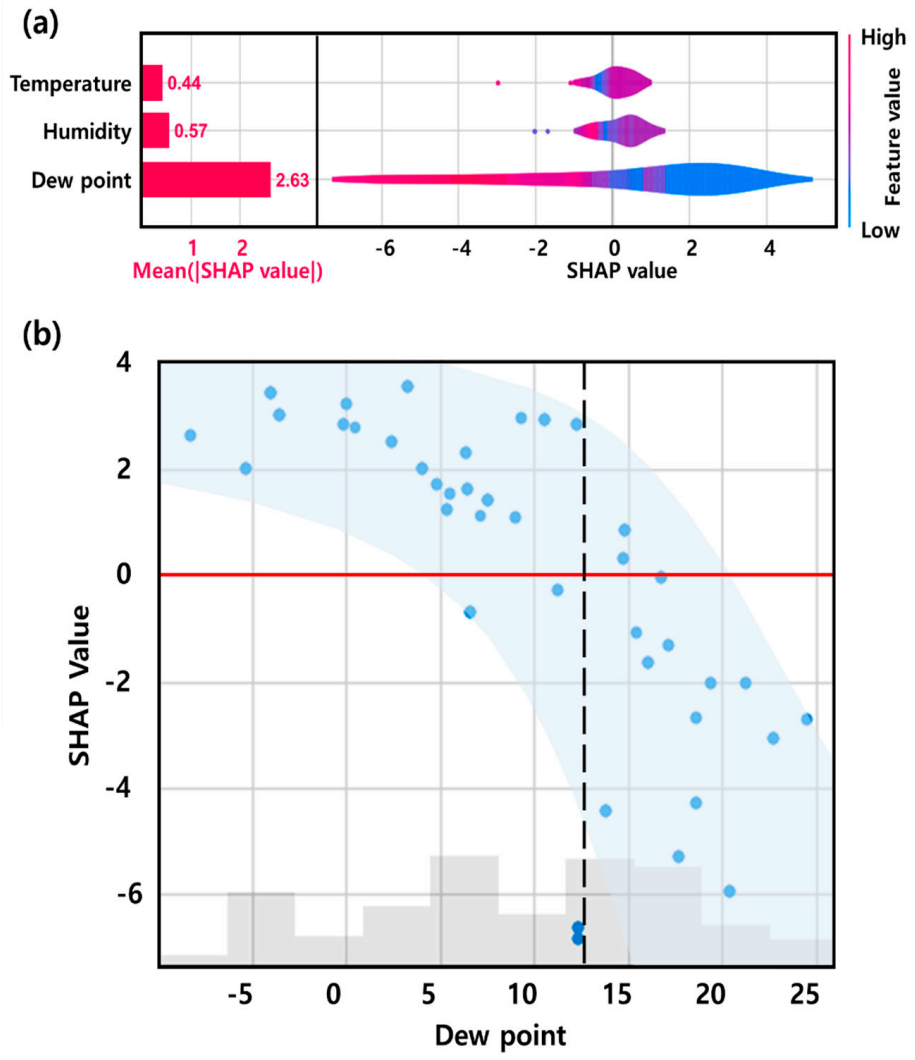

Figure 5. (**a**) Feature importance in the model. Dew point shows the highest feature importance, suggesting that dew point is the crucial factor with a substantial impact on efficiency. (**b**) Relationship between SHAPs values and dew points. Blue background region implies the trend of the obtained data points. The point where SHAP is zero is indicated with a red line, and the dashed line indicates the criteria for dew point suggested in this work that exhibits a positive SHAP value.

4. Conclusions

In this study, we developed a machine learning model to predict the efficiency of ambient-processed perovskite solar cells based on the dew point. A total of 238 perovskite solar cells were fabricated, and their photovoltaic parameters were collected along with the dew points at the time of fabrication. We observed a correlation where devices fabricated in high-dew-point environments exhibited lower efficiency. Using the SCAPS-1D simulation program, we indirectly confirmed that the dew point influenced the perovskite layer during fabrication.

Various tree-based models (DT, ET, RF, GB, and AdaBoost) were applied for comparative analysis. The random forest model demonstrated the highest prediction accuracy for efficiency. Using the model trained with data from March to December 2023, efficiency predictions for January and February 2024 were made, achieving a MPAE of 4.44%; this underscores the model's capability to accurately predict the efficiency of perovskite solar cell fabricated in an ambient atmosphere with a dew point.

Certainly, there are regional and seasonal differences among laboratories, as well as variations in perovskite fabrication methods such as whether additives are used. Therefore, it could be challenging to expect the same level of prediction accuracy if the data points obtained in our laboratory were applied in other laboratories. In addition, considering the numerous variables present in the ambient environment, there may be other potential environmental factors that are not considered in this study. Although every effort was made to ensure that the experiment processes (substrate cleaning, precursor solution synthesis, and measurements) were performed under strictly identical conditions, factors such as total duration of exposure to the ambient environment until device fabrication is completed, the shelf life of materials, and barometric pressure which varies with altitude may also influence the device performance. Nevertheless, the methodology proposed in this study using the dew point holds significant potential for predicting the efficiency of ambient-processed perovskite solar cells. It becomes possible to reliably predict the efficiency of perovskite solar cells fabricated in ambient conditions, which could serve as a guideline for future cell production under similar conditions. Moreover, the methodology applied in this work offers the following additional directions for future development:

(1) From an industry perspective, the model could assist in optimizing production output. Variations in perovskite solar cell efficiency under ambient conditions are closely linked to production reliability, which, in turn, can significantly impact overall production yields. Since the issue of the stability of perovskite solar cells being influenced by environmental factors remains unresolved, employing this model to predict efficiencies in advance and adjust production output represents a practical and effective solution. Moreover, this capability is anticipated to play a pivotal role in enabling the implementation of smart factory systems, which are defined by autonomous and adaptive production processes.

(2) The methodology can be applied to various compositions of perovskite solar cells, not only for $MAPbI_3$. Appling the same methodology to various compositions is expected to provide more reliable and comprehensive results. Furthermore, this approach has the potential to go beyond predicting cell efficiency, extending to forecasts of module-level power output and establishing a framework for comprehensive predictive tools applicable across the industry.

(3) If this methodology were applied in reverse, it could aid in developing perovskite solar cells that are more resistant to environmental factors. Once this model is expanded to accommodate various types of perovskite solar cells, it could be utilized to identify cell types that exhibit the least sensitivity to changes in environmental conditions by varying environmental parameters and analyzing the corresponding machine learning predictions. This indicates that the model could also play a pivotal role in proposing optimized compositions, materials, and structural designs for perovskite solar cells. Such applications would further contribute to advancing research on the stability of perovskite solar cells.

Considering all of these points, the model and methodology proposed in this work are expected to make a significant contribution to the advancement of commercialization and upscaling of perovskite solar cells in the future.

Supplementary Materials: The following supporting information can be downloaded at: https://www.mdpi.com/article/10.3390/en17235998/s1, Figure S1: Perovskite film fabricated under different relative humidity conditions, Figure S2: Obtaining the meteorological data of the laboratory using a thermohygrometer, Figure S3: Correlation between two different dew points, Figure S4. Prediction results using the randon forest model, Figure S5. Validation of the SHAP-derived dew point threshold, Table S1: Input parameters used in SCAPS-1D simulation.

Author Contributions: D.P., S.L. (Seungtae Lee) and S.L. (Solhee Lee) contributed equally to this work. Conceptualization, D.P., S.L. (Seungtae Lee) and S.L. (Solhee Lee); methodology, D.P. and S.L. (Solhee Lee); validation, S.L. (Solhee Lee); formal analysis, S.-H.J. and S.L. (Solhee Lee); investigation, D.P. and J.-K.H.; resources, S.L. (Sangwon Lee), J.-K.H., J.N. and K.K.; data curation, K.K., Y.K. (Youngmin Kim), S.C., J.-S.H. and W.L.; writing—original draft preparation, D.P. and S.L. (Seungtae Lee); writing—review and editing, D.P. and S.L. (Seungtae Lee); visualization, D.P. and S.L. (Seungtae Lee); supervision, D.K. and Y.K. (Yoonmook Kang); project administration, D.K. and Y.K. (Yoonmook Kang); funding acquisition, H.-S.L. and D.K. All authors have read and agreed to the published version of the manuscript.

Funding: This work was supported by the "Human Resources Program in Energy Technology" of the Korea Institute of Energy Technology Evaluation and Planning (KETEP), granted financial resources from the Ministry of Trade, Industry &Energy, Republic of Korea (No. 20204010600470). This work was supported by the Korea Institute of Energy Technology Evaluation and Planning (KETEP) from the Ministry of Trade, Industry, and Energy (20214000000680).

Data Availability Statement: The original contributions presented in the study are included in the article, further inquiries can be directed to the corresponding author.

Conflicts of Interest: The authors declare no conflicts of interest.

References

1. Min, H.; Lee, D.Y.; Kim, J.; Kim, G.; Lee, K.S.; Kim, J.; Paik, M.J.; Kim, Y.K.; Kim, K.S.; Kim, M.G. Perovskite solar cells with atomically coherent interlayers on SnO_2 electrodes. *Nature* **2021**, *598*, 444–450. [CrossRef] [PubMed]
2. Noh, J.H.; Im, S.H.; Heo, J.H.; Mandal, T.N.; Seok, S.I. Chemical management for colorful, efficient, and stable inorganic–organic hybrid nanostructured solar cells. *Nano Lett.* **2013**, *13*, 1764–1769. [CrossRef] [PubMed]
3. Yin, W.-J.; Yang, J.-H.; Kang, J.; Yan, Y.; Wei, S.-H. Halide perovskite materials for solar cells: A theoretical review. *J. Mater. Chem. A* **2015**, *3*, 8926–8942. [CrossRef]
4. Kojima, A.; Teshima, K.; Shirai, Y.; Miyasaka, T. Organometal halide perovskites as visible-light sensitizers for photovoltaic cells. *J. Am. Chem. Soc.* **2009**, *131*, 6050–6051. [CrossRef] [PubMed]
5. NREL. Best Research-Cell Efficiencies. Available online: https://www.nrel.gov/pv/assets/pdfs/best-research-cell-efficiencies.pdf (accessed on 10 November 2023).
6. Al-Ashouri, A.; Köhnen, E.; Li, B.; Magomedov, A.; Hempel, H.; Caprioglio, P.; Márquez, J.A.; Morales Vilches, A.B.; Kasparavicius, E.; Smith, J.A. Monolithic perovskite/silicon tandem solar cell with >29% efficiency by enhanced hole extraction. *Science* **2020**, *370*, 1300–1309. [CrossRef]
7. Chen, B.; Zhengshan, J.Y.; Manzoor, S.; Wang, S.; Weigand, W.; Yu, Z.; Yang, G.; Ni, Z.; Dai, X.; Holman, Z.C. Blade-coated perovskites on textured silicon for 26%-efficient monolithic perovskite/silicon tandem solar cells. *Joule* **2020**, *4*, 850–864. [CrossRef]
8. Hyun, J.Y.; Yeom, K.M.; Lee, S.-W.; Bae, S.; Choi, D.; Song, H.; Kang, D.; Hwang, J.-K.; Lee, W.; Lee, S. Perovskite/Silicon Tandem Solar Cells with a V_{oc} of 1784 mV Based on an Industrially Feasible 25 cm^2 TOPCon Silicon Cell. *ACS Appl. Energy Mater.* **2022**, *5*, 5449–5456. [CrossRef]
9. Pyun, D.; Lee, S.-W.; Kim, Y.; Jang, G.S.; Choi, D.; Jeong, S.H.; Song, H.; Lee, S.; Cho, S.; Kim, J. First Demonstration of Top Contact-Free Perovskite/Silicon Two-Terminal Tandem Solar Cells for Overcoming the Current Density Hurdle. *ACS Appl. Energy Mater.* **2023**, *6*, 2687–2697. [CrossRef]
10. Pyun, D.; Choi, D.; Bae, S.; Lee, S.-W.; Song, H.; Jeong, S.H.; Lee, S.; Hwang, J.-K.; Cho, S.; Lee, H. Titanium Silicide: A Promising Candidate of Recombination Layer for Perovskite/Tunnel Oxide Passivated Contact Silicon Two-Terminal Tandem Solar Cells. *ACS Appl. Mater. Interfaces* **2024**, *16*, 28379–28390. [CrossRef] [PubMed]
11. Jeong, S.-H.; Hwang, J.-S.; Hwang, J.-K.; Lee, S.-W.; Lee, W.; Lee, S.; Pyun, D.; Cho, S.; Choe, Y.; Lee, H.-S. Potassium chloride passivation for sputtered SnO_2 to eliminate hysteresis and enhance the efficiency of perovskite solar cells. *J. Alloys Compd.* **2023**, *968*, 171890. [CrossRef]

12. Bae, M.-S.; Chang, Y.H.; Li, M.Q.; Kim, S.-W.; Lee, W.; Bae, J.-J.; Kim, D.; Kim, H.-S.; Lim, J.; Lee, J. Enhanced chemical interaction between ionic liquid and halide perovskite to improve performance of perovskite solar cells. *Mater. Today Energy* **2024**, *43*, 101593. [CrossRef]
13. Hwang, J.-K.; Jeong, S.-H.; Kim, D.; Lee, H.-S.; Kang, Y. A Review on Dry Deposition Techniques: Pathways to Enhanced Perovskite Solar Cells. *Energies* **2023**, *16*, 5977. [CrossRef]
14. Kim, B.-S.; Pérez-del-Rey, D.; Paliwal, A.; Dreessen, C.; Sessolo, M.; Bolink, H.J. Simple approach for an electron extraction layer in an all-vacuum processed nip perovskite solar cell. *Energy Adv.* **2022**, *1*, 252–257. [CrossRef] [PubMed]
15. Hwang, J.-K.; Lee, S.-W.; Lee, W.; Bae, S.; Kang, D.; Jeong, S.-H.; Lee, S.; Pyun, D.; Hwang, J.-S.; Cho, S. Sputtered PbI_2 with Post-Processing for Perovskite Solar Cells. *Solar RRL* **2023**, *7*, 2300214. [CrossRef]
16. Lee, J.; Kang, H.; Kim, G.; Back, H.; Kim, J.; Hong, S.; Park, B.; Lee, E.; Lee, K. Achieving large-area planar perovskite solar cells by introducing an interfacial compatibilizer. *Adv. Mater.* **2017**, *29*, 1606363. [CrossRef]
17. Kim, S.-W.; Moon, S.J.; Kim, S.-H.; Yoo, J.J.; Kim, D.; Kim, B.-S.; Jeon, N.J. Reducing Humidity Dependency of Ambient-Air-Processed Wide-Bandgap Inverted Perovskite Solar Cells. *ACS Energy Lett.* **2023**, *8*, 4777–4781. [CrossRef]
18. Yan, L.; Huang, H.; Cui, P.; Du, S.; Lan, Z.; Yang, Y.; Qu, S.; Wang, X.; Zhang, Q.; Liu, B. Fabrication of perovskite solar cells in ambient air by blocking perovskite hydration with guanabenz acetate salt. *Nat. Energy* **2023**, *8*, 1158–1167. [CrossRef]
19. Zeng, Q.; Ma, Q.; Li, L.; Zheng, B.; Pan, Y.; Zhao, X.; Xiao, H.; Yan, C.; Liu, F. Tailoring particle size of PbI_2 towards efficient perovskite solar cells under ambient air conditions. *Chem. Commun.* **2023**, *59*, 5269–5272. [CrossRef] [PubMed]
20. Zheng, X.; Kong, W.; Wen, J.; Hong, J.; Luo, H.; Xia, R.; Huang, Z.; Luo, X.; Liu, Z.; Li, H. Solvent engineering for scalable fabrication of perovskite/silicon tandem solar cells in air. *Nat. Commun.* **2024**, *15*, 4907. [CrossRef]
21. Ghosh, S.; Boro, B.; Porwal, S.; Mishra, S.; Singh, T. Role of antisolvent temperature and quaternary ammonium cation-based ionic liquid engineering in the performance of perovskite solar cells processed under air ambient conditions. *Energy Adv.* **2023**, *2*, 1155–1165. [CrossRef]
22. Boro, B.; Mishra, S.; Singh, P.; Lahiri, B.; Varshney, S.K.; Singh, T. Thermal Stability Analysis of Formamidinium–Cesium-Based Lead Halide Perovskite Solar Cells Fabricated under Air Ambient Conditions. *Energy Technol.* **2024**, *12*, 2400034. [CrossRef]
23. Mesquita, I.; Andrade, L.; Mendes, A. Effect of relative humidity during the preparation of perovskite solar cells: Performance and stability. *Solar Energy* **2020**, *199*, 474–483. [CrossRef]
24. Berhe, T.A.; Su, W.-N.; Chen, C.-H.; Pan, C.-J.; Cheng, J.-H.; Chen, H.-M.; Tsai, M.-C.; Chen, L.-Y.; Dubale, A.A.; Hwang, B.-J. Organometal halide perovskite solar cells: Degradation and stability. *Energy Environ. Sci.* **2016**, *9*, 323–356. [CrossRef]
25. Lee, S.-W.; Kim, S.; Bae, S.; Cho, K.; Chung, T.; Mundt, L.E.; Lee, S.; Park, S.; Park, H.; Schubert, M.C. UV degradation and recovery of perovskite solar cells. *Sci. Rep.* **2016**, *6*, 38150. [CrossRef] [PubMed]
26. Hsu, R.-Y.; Liang, Y.-J.; Hung, Y.-J.; Lin, Y.-C. Impact of humidity in triple cation perovskite solar cells: Surface analysis. *Mater. Sci. Semicond. Process.* **2022**, *152*, 107100. [CrossRef]
27. Purev-Ochir, B.; Liu, X.; Fujita, Y.; Semba, D.; Raju, T.B.; Tumen-Ulzii, G.; Wachi, A.; Sato, H.; Matsushima, T.; Adachi, C. Oxygen-Induced Reversible Degradation of Perovskite Solar Cells. *Solar RRL* **2023**, *7*, 2300127. [CrossRef]
28. Cheng, Y.; Li, H.-W.; Qing, J.; Yang, Q.-D.; Guan, Z.; Liu, C.; Cheung, S.H.; So, S.K.; Lee, C.-S.; Tsang, S.-W. The detrimental effect of excess mobile ions in planar $CH_3NH_3PbI_3$ perovskite solar cells. *J. Mater. Chem. A* **2016**, *4*, 12748–12755. [CrossRef]
29. Manspeaker, C.; Merrion, G.; Krouse, K.; Zakhidov, A. Ambient processing conditions and their effects on perovskite device performance. *Cryst. Res. Technol.* **2022**, *57*, 2100116. [CrossRef]
30. Toloueinia, P.; Khassaf, H.; Shirazi Amin, A.; Tobin, Z.M.; Alpay, S.P.; Suib, S.L. Moisture-induced structural degradation in methylammonium lead iodide perovskite thin films. *ACS Appl. Energy Mater.* **2020**, *3*, 8240–8248. [CrossRef]
31. Howard, J.M.; Wang, Q.; Srivastava, M.; Gong, T.; Lee, E.; Abate, A.; Leite, M.S. Quantitative predictions of moisture-driven photoemission dynamics in metal halide perovskites via machine learning. *J. Phys. Chem. Lett.* **2022**, *13*, 2254–2263. [CrossRef] [PubMed]
32. Srivastava, M.; Hering, A.R.; An, Y.; Correa-Baena, J.-P.; Leite, M.S. Machine learning enables prediction of halide perovskites' optical behavior with >90% accuracy. *ACS Energy Lett.* **2023**, *8*, 1716–1722. [CrossRef] [PubMed]
33. Mammeri, M.; Bencherif, H.; Dehimi, L.; Hajri, A.; Sasikumar, P.; Syed, A.; AL-Shwaiman, H.A. Stability forecasting of perovskite solar cells utilizing various machine learning and deep learning techniques. *J. Opt.* **2024**, *1*, 1–9. [CrossRef]
34. Ko, Y.; Lee, C.; Kim, Y.; Kim, Y.; Yun, Y.J.; Jun, Y. Dew point temperature as an invariant replacement for relative humidity for advanced perovskite solar cell fabrication systems. *J. Mater. Chem. A* **2018**, *6*, 20695–20701. [CrossRef]
35. Kim, S.; Bae, S.; Lee, S.-W.; Cho, K.; Lee, K.D.; Kim, H.; Park, S.; Kwon, G.; Ahn, S.-W.; Lee, H.-M. Relationship between ion migration and interfacial degradation of $CH_3NH_3PbI_3$ perovskite solar cells under thermal conditions. *Sci. Rep.* **2017**, *7*, 1200. [CrossRef] [PubMed]
36. Bae, S.; Kim, S.; Lee, S.-W.; Cho, K.J.; Park, S.; Lee, S.; Kang, Y.; Lee, H.-S.; Kim, D. Electric-field-induced degradation of methylammonium lead iodide perovskite solar cells. *J. Phys. Chem. Lett.* **2016**, *7*, 3091–3096. [CrossRef] [PubMed]
37. Burst, J.M.; Duenow, J.N.; Albin, D.S.; Colegrove, E.; Reese, M.O.; Aguiar, J.A.; Jiang, C.-S.; Patel, M.; Al-Jassim, M.M.; Kuciauskas, D. CdTe solar cells with open-circuit voltage breaking the 1 V barrier. *Nat. Energy* **2016**, *1*, 16015. [CrossRef]
38. Scarpulla, M.A.; McCandless, B.; Phillips, A.B.; Yan, Y.; Heben, M.J.; Wolden, C.; Xiong, G.; Metzger, W.K.; Mao, D.; Krasikov, D. CdTe-based thin film photovoltaics: Recent advances, current challenges and future prospects. *Sol. Energy Mater. Sol. Cells* **2023**, *255*, 112289. [CrossRef]

39. Kartopu, G.; Oklobia, O.; Turkay, D.; Diercks, D.; Gorman, B.; Barrioz, V.; Campbell, S.; Major, J.; Al Turkestani, M.; Yerci, S. Study of thin film poly-crystalline CdTe solar cells presenting high acceptor concentrations achieved by in-situ arsenic doping. *Sol. Energy Mater. Sol. Cells* **2019**, *194*, 259–267. [CrossRef]
40. Ablekim, T.; Colegrove, E.; Metzger, W.K. Interface engineering for 25% CdTe solar cells. *ACS Appl. Energy Mater.* **2018**, *1*, 5135–5139. [CrossRef]
41. Wang, Y.; Dar, M.I.; Ono, L.K.; Zhang, T.; Kan, M.; Li, Y.; Zhang, L.; Wang, X.; Yang, Y.; Gao, X. Thermodynamically stabilized β-$CsPbI_3$–based perovskite solar cells with efficiencies >18%. *Science* **2019**, *365*, 591–595. [CrossRef]
42. Chen, H.; Fu, W.; Huang, C.; Zhang, Z.; Li, S.; Ding, F.; Shi, M.; Li, C.Z.; Jen, A.K.Y.; Chen, H. Molecular engineered hole-extraction materials to enable dopant-free, efficient p-i-n perovskite solar cells. *Adv. Energy Mater.* **2017**, *7*, 1700012. [CrossRef]
43. Chouhan, A.S.; Jasti, N.P.; Avasthi, S. Effect of interface defect density on performance of perovskite solar cell: Correlation of simulation and experiment. *Mater. Lett.* **2018**, *221*, 150–153. [CrossRef]
44. Cai, Q.; Lin, Z.; Zhang, W.; Shen, G.; Wen, X.; Dong, H.; Xu, X.; Zhu, D.; Mu, C. Improvement performance of planar perovskite solar cells by bulk and surface defect passivation. *ACS Sustain. Chem. Eng.* **2021**, *9*, 13001–13009. [CrossRef]
45. Burgelman, M.; Nollet, P.; Degrave, S. Modelling polycrystalline semiconductor solar cells. *Thin Solid Film.* **2000**, *361*, 527–532. [CrossRef]
46. Abnavi, H.; Maram, D.K.; Abnavi, A. Performance analysis of several electron/hole transport layers in thin film $MAPbI_3$-based perovskite solar cells: A simulation study. *Opt. Mater.* **2021**, *118*, 111258. [CrossRef]
47. Grinsztajn, L.; Oyallon, E.; Varoquaux, G. Why do tree-based models still outperform deep learning on typical tabular data? *Adv. Neural Inf. Process. Syst.* **2022**, *35*, 507–520.
48. Scott, M.; Su-In, L. A unified approach to interpreting model predictions. *Adv. Neural Inf. Process. Syst.* **2017**, *30*, 4765–4774.
49. Lundberg, S.M.; Erion, G.; Chen, H.; DeGrave, A.; Prutkin, J.M.; Nair, B.; Katz, R.; Himmelfarb, J.; Bansal, N.; Lee, S.-I. From local explanations to global understanding with explainable AI for trees. *Nat. Mach. Intell.* **2020**, *2*, 56–67. [CrossRef]
50. Lee, M.-H. Interpretable machine-learning for predicting power conversion efficiency of non-halogenated green solvent-processed organic solar cells based on Hansen solubility parameters and molecular weights of polymers. *Sol. Energy* **2023**, *261*, 7–13. [CrossRef]